Micromechanical characterisation of overburden shales in the Horn River Basin through nanoindentation

IOP Conf. Series: Earth and Environmental Science 1124 (2023) 012087 doi:10.1088/1755-1315/1124/1/012087

Micromechanical characterisation of overburden shales in the Horn River Basin through nanoindentation

T S Charlton[1], M Rouainia[1], A C Aplin[2], Q J Fisher[3], L Bowen[4]

[1] School of Engineering, Newcastle University, Newcastle upon Tyne, NE1 7RU, UK
[2] Department of Earth Sciences, Durham University, Durham, DH1 3LE, UK
[3] School of Earth and Environment, University of Leeds, Leeds, LS2 9JT, UK
[4] Department of Physics, Durham University, Durham, DH1 3LE, UK

tom.charlton@newcastle.ac.uk

Abstract. The paper presents a micromechanical characterisation of Fort Simpson shale, which overlies unconventional gas-producing lithologies in the Horn River Basin, NW Canada. The Fort Simpson formation is clay-rich and microseismic data recorded during hydraulic fracturing events in the underlying reservoir has shown the formation acts as a barrier to fracture development, with a notably anisotropic seismic response. Samples were prepared from core fragments and the composition and texture of the shale was characterised using X-ray diffraction, mercury injection porosimetry and scanning electron microscopy (SEM). Nanoindentation testing was used to obtain the mechanical response of the shale microstructure, at grain-scale. The indentation was conducted on a grid pattern and samples were oriented both parallel and perpendicular to the bedding plane to assess the inherent mechanical anisotropy. Chemical analysis of the grids was also undertaken through SEM/EDS (energy dispersive X-ray spectroscopy) and the coupled chemo-mechanical data was used to characterise the material phases of the shale through a statistical clustering procedure. The results show that Fort Simpson shale broadly consists of a soft clay phase, with strongly anisotropic elastic stiffness, and stiffer but effectively isotropic grains of quartz and feldspar. A simple upscaling scheme was also applied to link the grain-scale elastic stiffness to the field-scale microseismic data.

1. Introduction

The global drive towards net zero carbon emissions has led to a rapidly growing interest in subsurface technologies such as geological storage of CO_2, storing energy underground in the form of hydrogen and compressed air, and construction of nuclear waste repositories. At the same time, natural gas is often seen as an important 'transition fuel', and unconventional production is expected to continue to be an important supply over the next decade [1]. Shales, describing fine-grained sedimentary rocks of variable mineralogy, represent important components of these future energy and decarbonisation systems. They act as reservoirs for unconventional gas production and, crucially, serve as subsurface seals due to their low matrix permeability, preventing fluid flow and leakage. Both applications require knowledge on the geomechanical properties of shale, in order to predict how they will behave under elevated pressure.

Obtaining geomechanical properties, such as Young's modulus and compressive/tensile strength, has generally relied upon inference from wireline logs or, ideally, testing recovered core. Core through shale units has been infrequently collected during conventional oil and gas projects [2] and even where core is recovered, extracting good-quality shale samples sufficient for standard mechanical tests is a

significant challenge due to its often laminated and friable nature. Moreover, neither wireline logs nor core tests (due to sample preparation demands) allow for straightforward characterisation of anisotropy, which can be significant in shales and is important when interpreting seismic reflection data [3]. Inevitably, robust geomechanical data on shale lithologies tends to be sparse.

Since the mid-2000s, researchers have begun to investigate the mechanical properties of the shale constituents, the grains of phyllosilicates, quartz, feldspar, carbonates, organic matter and pyrite that variously make up the micro-composite shale material. The microstructure is significantly heterogeneous and the scale of the shale 'building blocks' ranges from sub-micron sized clay plates to lenses and particles of organic material at a few microns across to silt-size minerals. The experimental methods have included nanoindentation testing [4-7] and atomic force microscopy (AFM) [7, 8]. These micromechanical tests can be conducted on small pieces of shale, such as drill cuttings, instead of relying on intact cores; this also facilitates characterisation of anisotropy. Correlations between mineralogy and macroscopic mechanical properties have been reported [9] and the bulk mineralogy often determines the phase contributions in homogenisation models, where the aim is to fill the gaps in core-scale data by upscaling from the mechanical properties of the shale constituents [5, 7, 10].

This paper presents a robust micromechanical characterisation of the Fort Simpson shale, which overlies unconventional gas-producing lithologies in the Horn River Basin. First, the samples are characterised in terms of mineralogy, porosity and texture. Then, nanoindentation testing is coupled with chemical analyses and the chemo-mechanical data is used to constrain the behaviour of the individual material phases. Finally, an upscaling scheme is applied to predict the elastic properties and anisotropy of the shale composite and this is compared to microseismic data collected during hydraulic fracturing operations in the reservoir.

2. Sample characterisation

The Horn River Basin is located in north east British Columbia, Canada. It covers an area of approximately 12,000 km^2 in the northwestern part of the Western Canadian Sedimentary Basin where predominately carbonate and marine shales were deposited in the Middle and Late Devonian [11]. The Horn River shale sequence comprising the Evie and Otter Park Members of the Horn River Formation and the Muskwa Formation (Figure 1b) has been exploited for unconventional gas production [12] and the members range in thickness from 30 to 240m [13]. This sequence is underlain by the shallow water carbonates of the Keg River Formation and overlain by the argillaceous shale of the Fort Simpson Formation, which reaches thicknesses of over 1000m.

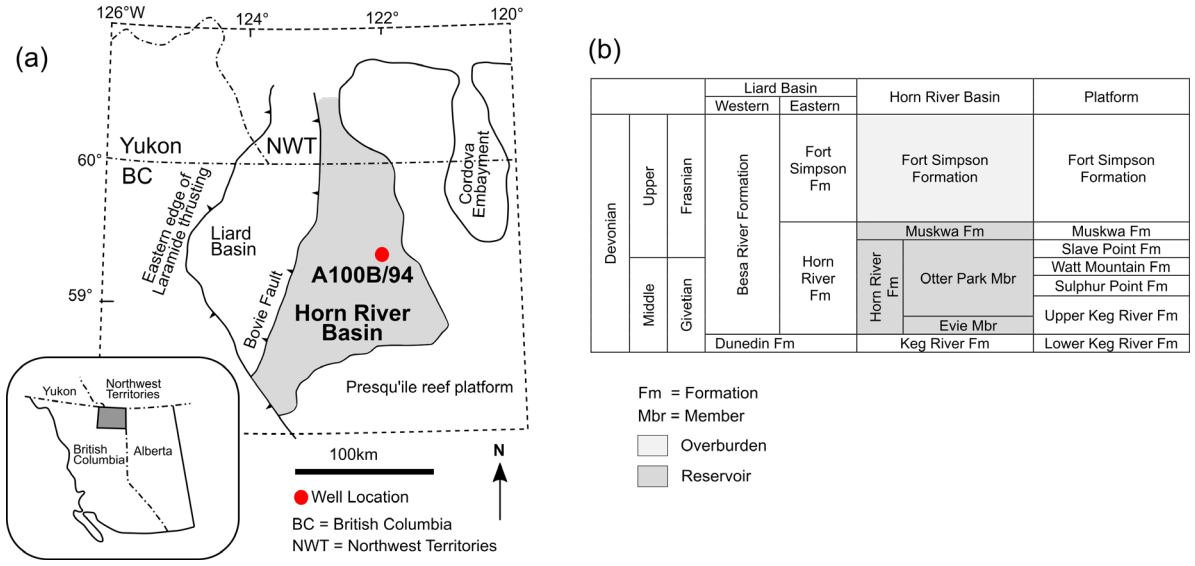

Figure 1. (a) Map of Horn River Basin showing well A100B/94; inset: map showing location of Horn River area in western Canada; (b) Middle and Upper Devonian stratigraphy. Modified from [11].

2.1. Composition

The focus of this paper is the overlying Fort Simpson Formation, which has been shown to perform as an effective fracture barrier in hydraulic fracturing operations [12]. Core was obtained from a well (A100B/94) drilled in the eastern part of the basin (see Figure 1a). Two samples were taken (from depths 2537.4m and 2542.2m, approximately 50m above the Muskwa Formation), and their bulk composition assessed by X-Ray Diffraction (XRD) and combustion for total organic carbon (TOC). Mercury injection capillary pressure (MICP) was used to estimate porosity.

Table 1 shows the bulk composition of the sample in terms of volume percent (vol%). This is converted from the measured weight percentages using standard grain densities [14]: quartz 2.65; albite 2.63; dolomite 2.87; siderite 3.96; pyrite 5.02; clay minerals from 2.42-2.75 (all in g/cm^3). Given the gas window maturity, the density of organic matter (OM) was taken as 1.35 g/cm^3 [7]. The data shows that the samples are clay-rich (>50%), with the clay fraction dominated by illite and illite-smectite. The Fort Simpson formation is known to be poor in organic matter [13] and the samples considered here have OM around 2%. Silt particles are mostly quartz, with small amounts of feldspar (albite), pyrite, and carbonates (dolomite and siderite). Porosity measured by MICP is less than 2%; this is similar to values reported by Ross and Bustin [13] on Fort Simpson samples also using MICP.

Table 1. Sample composition (vol%).

Sample	Quartz	Albite	Dolomite	Siderite	Pyrite	Clay	OM	Porosity
A3	26.6	4.5	-	0.7	0.9	63.1	2.5	1.7
A6	31.4	5.7	2.6	1.6	1.2	54.2	1.8	1.4

2.2. Microstructure

The texture of the Fort Simpson shale was analysed by scanning electron microscopy (SEM). Figure 2 shows images of the sample microstructures, taken in back-scattered electron (BSE) mode. Sample A3 has a very fine-grained matrix with small amounts of siderite and framboidal pyrite visible (Figure 2a). Figure 2b clearly shows a very strong orientation of the clay minerals in the porous matrix with scattered quartz grains. Sample A6 shows a similar texture (Figure 2c), dominated by a clay matrix with inclusions of framboidal pyrite and siderite. This sample also has a noticeable dolomite content, evident as individual grains scattered in the matrix, and the quartz content is generally coarser compared to A3. Figure 2d reveals that the clay minerals are less clearly aligned compared with the strongly oriented minerals in A3.

3. Nanoindentation and chemo-mechanical coupling

3.1. Method

Nanoindentation testing was carried out using a NanoTest Vantage system to investigate the mechanical response of the shale at a microstructural level. Samples were cut both parallel and perpendicular to the bedding plane and the sections were prepared by broad ion beam (BIB) polishing to minimise surface roughness. A diamond Berkovich indenter was pushed into the samples to a 'low' maximum load (F_{max}) of 5 mN, selected so that the indentation measures the response of the individual constituents. In contrast, a 'high' load (~250-500 mN) would measure a homogenised response [7]. The load was held at F_{max} for 60s to allow system equilibrium and to investigate the creep response (not reported here). The indentation (reduced) modulus, E^*, and hardness, H, are extracted from the loading and unloading curves. The indentation was conducted on 15 × 15 grids, with indents spaced 5 μm apart given expected displacements of less than one micron.

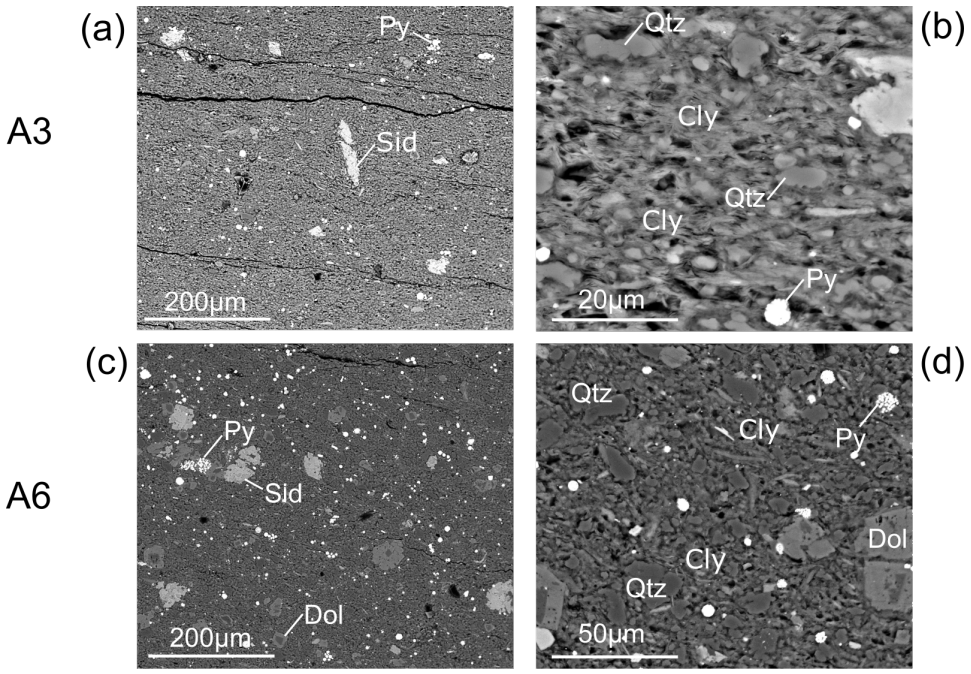

Figure 2. BSE images. (a) and (b) Fort Simpson sample A3: illite-dominated clay (Cly) matrix with dispersed grains of quartz (Qtz), pyrite (Py) and siderite (Sid); (c) and (d) Fort Simpson sample A6: similar texture to A3 but less strongly aligned clay minerals and with presence of dolomite (Dol) grains.

Interpretation of nanoindentation testing generally relies on statistical approaches due to the 'big data' nature of massive grid indentation campaigns. Coupling chemical testing with mechanical nanoindentation data can improve the identification of significant material phases in the shale composite [15]. This is particularly important when the geomechanical properties are linked to upscaling schemes: a more robust characterisation of the fundamental micromechanics allows a better prediction of properties obtained at larger scales, including quantification of uncertainty in the measured properties. To this end, SEM-EDS was conducted on each of the nanoindentation grids (post-indentation) and a Gaussian mixture model (GMM) used to extract the mechanical properties of the material phases from the coupled chemo-mechanical data. The GMM procedure implemented in Matlab was applied, in which likelihood is optimised using the iterative expectation-maximization algorithm.

3.2. Results

The mechanical results obtained from the nanoindentation testing are shown in Figure 3. The load displacement curves (Figures 3a and c) show typical load-hold-unload phases and the maximum displacement is generally less than 800 nm, aside from three indents on sample A3 where h_{max} reaches 1 µm. Curves showing significant 'pop-in' behaviour, relating to particle breakage and flaking, have been removed from the current analysis. It is evident from the load-displacement curves that there is a different response in directions parallel (direction-1) and perpendicular (direction-3) to the bedding plane (see image inset in Figure 3b for a schematic illustration of each direction in relation to the bedding). In particular, samples indented perpendicular to the bedding plane tend to show a larger h_{max}, which is more evident on sample A3 than A6. This anisotropic response is also evident in Figures 3c and d, where the calculated indentation modulus and hardness are plotted for each indent. In general, a positive correlation is expected with E^* approximately proportional to $\sqrt{H}$ [4]. The nanoindentation data follows a positive correlation but the data tends to plot in groups, with the shale constituents having different mechanical signatures in terms of E^* and H. In the softer region ($E^* < 75$ GPa and $H < 5$ GPa), the clusters are likely to belong to the soft matrix phase of porous clay and organic matter, and it is notable that there is an obvious anisotropy with samples indented perpendicular to the bedding plane showing a softer response.

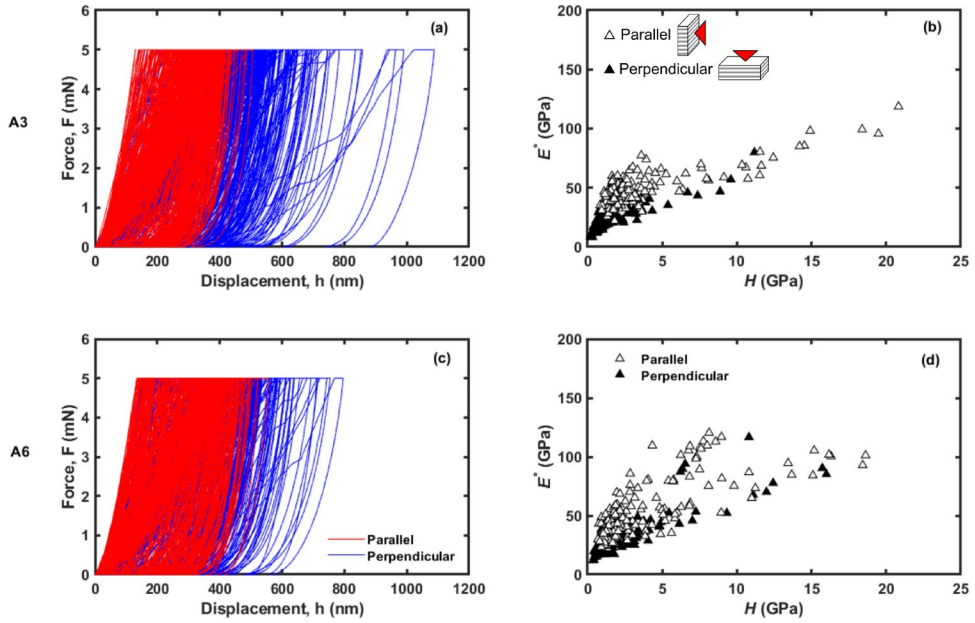

Figure 3. Load displacement curves and plots of indentation modulus (E^*) vs. hardness (H) on (a-b) A3 and (c-d) A6. Inset in (c): schematic of indentation directions (parallel to bedding plane and perpendicular to bedding plane).

Figure 4 shows SEM-EDS analysis of the nanoindentation grid on sample A6 (parallel). The chemical analysis reveals the distribution of material phases targeted by the nanoindentation grid: the matrix phyllosilicates are rich in Al and Si and quartz grains (high Si) are frequent inclusions, tending to be approx. 5 µm in size. The grid also falls on larger (~10-20 µm diameter), isolated grains of dolomite (high Ca and Mg). Framboidal pyrite (high Fe) and albite (high Na) appear as small particles, a few microns across.

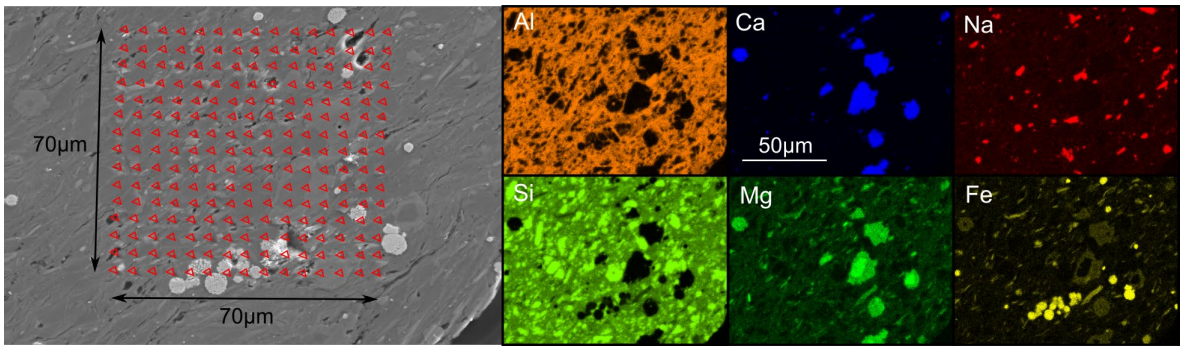

Figure 4. Left: BSE image of nanoindentation grid (indents marked on for clarity) on A6 (parallel). Right: EDS maps of the same area showing element composition.

The GMM was applied to the data in two steps. Firstly, the mechanical data (E^*, H) was fitted, using 10 replicates from different starting points with the minimum log-likelihood selected. Then, coupled chemo-mechanical data was considered, and the algorithm run starting from the results of step 1 (mechanical clustering). Taking sample A6 as an illustrative example, three material phases were assumed: a clay matrix, a quartz + feldspar phase, and dolomite inclusions. Figure 5 shows the results of the clustering approach using Al, Si and Ca intensity values. Using only mechanical data (Figure 5a), a soft phase is identified, which is likely to be the clay matrix, and two stiffer clusters are identified, separated in terms of hardness. Chemo-mechanical clustering (Figure 5b) identifies a very similar clay matrix (shown to be rich in Al and Si) but finds dolomite and quartz phases where both show E^* positively correlated with H.

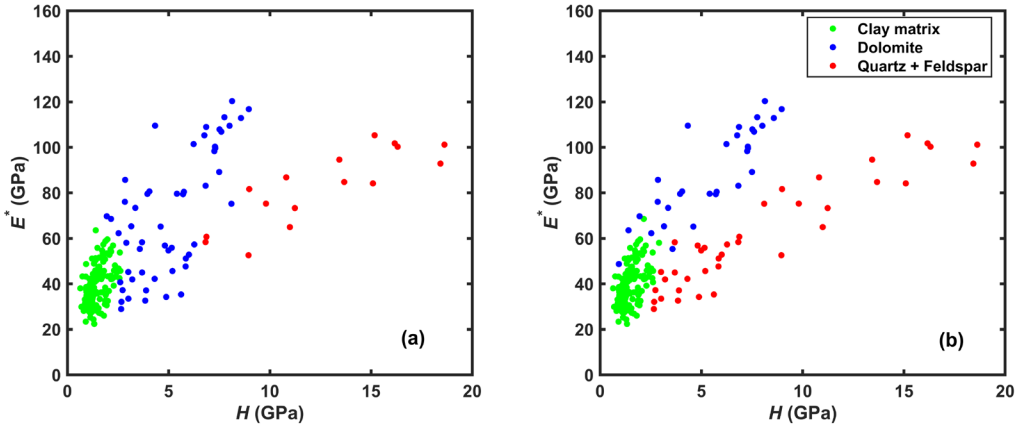

Figure 5. GMM clustering using (a) mechanical and (b) chemo-mechanical data on A6 (parallel).

The clusters are plotted on a composite EDS map in Figure 6 and are successfully located almost directly on the corresponding particles. The group of small pyrite framboids at the bottom of the grid cause some difficulty as the indents tend to fall at the grain edges. The GMM volume fractions (67% clay, 19% quartz + feldspar and 15% dolomite) are comparable to the bulk XRD but with a greater proportion of dolomite due to the grid being positioned on large dolomite grains. The mean stiffness properties of the clay phase on A6 are E_1^*= 40 and E_3^*= 22 GPa, compared to E_1^*= 43 and E_3^*= 19 GPa on A3, reflecting the stronger orientation observed in the SEM images of A3. Quartz/feldspar and dolomite show means around E^* = 60 and 87 GPa respectively and are effectively isotropic.

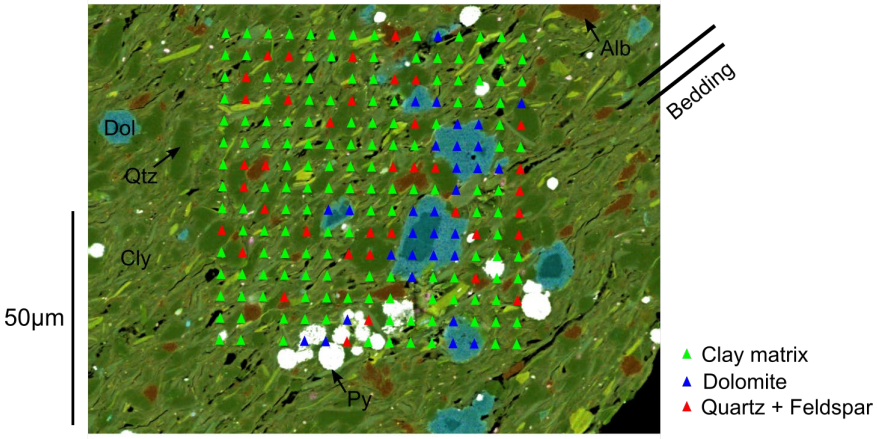

Figure 6. Composite EDS map of nanoindentation grid on A6 (parallel) showing GMM chemo-mechanical clusters. Alb: Albite; Cly: Clay matrix; Dol: Dolomite; Py: Pyrite; Qtz: Quartz.

4. Upscaling

4.1. Mean field homogenisation

Linear micromechanics can be used to homogenise the elastic response through various levels [16]. The homogenised stiffness tensor for a composite of N phases can be written:

$$\mathbb{C}_{hom} = \sum_{r=0}^{N} f_r \mathbb{C}_r : \mathbb{A}_r \quad (1)$$

where f_r is the volume fraction, $\mathbb{C}_r$ is the stiffness tensor, and $\mathbb{A}_r$ is the strain localisation tensor of the r-th phase which depends on the chosen homogenisation scheme. Two popular approaches are the Mori-Tanaka (MT) method and the Self-Consistent Scheme (SCS). For MT, the inclusions are embedded in a matrix while for SCS, the inclusions are inside the homogenised medium itself.

Figure 7 presents a conceptual model, similar to that of [7], for Fort Simpson shale and a two-step procedure to integrate the nanoindentation data. It is assumed that the micromechanical properties of the clay-rich phase belong to a matrix of clay, pores and OM (E_{OM} = 11GPa [7]); step 1 is a back analysis from the measured (anisotropic) indentation moduli to the transversely isotropic (TI) solid clay properties. The inversion is constrained by requiring realistic values of Poisson's ratio. Step 2 is then a forward model to predict the effect of (spherical, isotropic) inclusions of quartz/feldspar, carbonates (both stiffnesses measured in Section 3.2) and pyrite (E_{py} = 256 GPa) [Level II], and horizontal microcracks [Level III]. Microcracks are bedding parallel and have a density parameter d = 0.03.

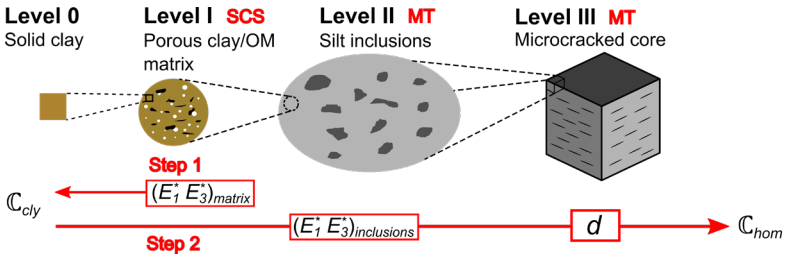

Figure 7. Conceptual multiscale model for Fort Simpson shale.

4.2. Comparison with microseismic data

Microseismic data from the Horn River Basin shows that the Fort Simpson shale has a very strong seismic anisotropy, with evidence of shear wave triplication; this response has been linked to the alignment of clay minerals and presence of aligned cracks [17]. Table 2 shows literature estimates of the Thomsen anisotropy parameters (ε, γ and δ) and vertical wave velocities, both of which are functions of the C_{ij} components of $\mathbb{C}_{hom}$, alongside the results from upscaling samples A3 and A6. In general, a good agreement is observed between the literature and upscaled values of both anisotropy parameters and wave velocities. Sample A3 shows very high anisotropy parameters due to its greater clay content relative to A6, in addition to a more anisotropic stiffness response of the matrix. For A3, $\mathbb{C}_{cly}$ has components C_{11} = 91.6, C_{12} = 48.2, C_{13} = 22.4, C_{33} = 29.0, and C_{44} = 5.1 GPa, which are very similar to those obtained by [18]. The ratio V_{P0} / V_{S0} tends to be slightly lower for the upscaled results than literature models. The inclusion of cracks at Level III increases the value of the anisotropy parameters but reduces V_{P0} / V_{S0}. Crack compliance and saturation may need to be considered for better predictions.

Table 2. Thomsen anisotropy parameters and seismic velocities of Fort Simpson shale from literature [17, 19, 20] and by upscaling micromechanical data.

		ε	γ	δ	V_{P0} (km/s)	V_{S0} (km/s)	V_{P0} / V_{S0}
Baird *et al.* [17]		0.33	0.46	0.01	3.38	1.65	2.05
ESG (in [17])		0.37	0.36	0.37	3.24	1.77	1.83
Yu and Shapiro [20]		0.38	0.69	0.19	3.50	1.60	2.19
Sayers *et al.* [19]		0.16	0.16	-0.005	3.80	1.86	2.04
A3	Level II	0.58	0.76	-0.03	3.48	1.80	1.93
	Level III	0.76	0.81	0.05	3.20	1.77	1.81
A6	Level II	0.30	0.44	-0.05	3.90	1.99	1.96
	Level III	0.44	0.48	0.02	3.58	1.95	1.84

5. Conclusions

This paper has reported some results of a micromechanical characterisation of the Fort Simpson shale formation which forms the overburden in the Horn River Basin. Low load nanoindentation testing was coupled with EDS chemical analysis to obtain the mechanical response of the shale constituents. The results show a significant mechanical anisotropy of the clay fabric of the Fort Simpson shale. A multi-level homogenisation scheme was used to upscale the micromechanical properties from grain to core-scale. A good comparison was observed between upscaled values of the Thomsen anisotropy parameters and wave velocities and estimates available in the literature from microseismic and wireline log data.

Acknowledgements
The authors would like to thank NERC for funding this research through the SHAPE-UK project (grant numbers NE/R018057/1, NE/R017840/1, and NE/R017565/1).

References

[1] International Energy Agency 2021 World Energy Outlook 2021.
[2] Worden R H, Allen M J, Faulkner D R, Utley J E P, Bond C E, Alcalde J, Heinemann N, Haszeldine R S, Mackay E and Ghanbari S 2020 Lower Cretaceous Rodby and Palaeocene Lista Shales: Characterisation and Comparison of Top-Seal Mudstones at Two Planned CCS Sites, Offshore UK *Minerals* **10** 691
[3] Sayers C M 2005 Seismic anisotropy of shales *Geophysical Prospecting* **53** 667-76
[4] Ulm F-J and Abousleiman Y 2006 The nanogranular nature of shale *Acta Geotechnica* **1** 77-88
[5] Ortega J A, Ulm F-J and Abousleiman Y 2007 The effect of the nanogranular nature of shale on their poroelastic behavior *Acta Geotechnica* **2** 155-82
[6] Graham S P, Rouainia M, Aplin A C, Cubillas P, Fender T D and Armitage P J 2021 Geomechanical characterisation of organic-rich calcareous shale using AFM and nanoindentation *Rock Mechanics and Rock Engineering* **54** 303-20
[7] Charlton T S, Goodarzi M, Rouainia M, Aplin A C and Cubillas P 2021 Effect of Diagenesis on Geomechanical Properties of Organic-Rich Calcareous Shale: A Multiscale Investigation *Journal of Geophysical Research: Solid Earth* **126** e2020JB021365
[8] Eliyahu M, Emmanuel S, Day-Stirrat R J and Macaulay C I 2015 Mechanical properties of organic matter in shales mapped at the nanometer scale *Marine and Petroleum Geology* **59** 294-304
[9] Sone H and Zoback M D 2013 Mechanical properties of shale-gas reservoir rocks — Part 1: Static and dynamic elastic properties and anisotropy *GEOPHYSICS* **78** D381-D92
[10] Goodarzi M, Rouainia M, Aplin A C, Cubillas P and de Block M 2017 Predicting the elastic response of organic-rich shale using nanoscale measurements and homogenisation methods *Geophysical Prospecting* **65** 1597-614
[11] Dong T, Harris N B, Ayranci K and Yang S 2017 The impact of rock composition on geomechanical properties of a shale formation: Middle and Upper Devonian Horn River Group shale, Northeast British Columbia, Canada *AAPG Bulletin* **101** 177-204
[12] BC Oil and Gas Commission 2014 Horn River Basin Unconventional Shale Gas Play Atlas.
[13] Ross D J K and Bustin R M 2008 Characterizing the shale gas resource potential of Devonian–Mississippian strata in the Western Canada sedimentary basin: Application of an integrated formation evaluation *AAPG Bulletin* **92** 87-125
[14] Mavko G, Mukerji T and Dvorkin J 2009 *The Rock Physics Handbook: Tools for Seismic Analysis of Porous Media* (Cambridge: Cambridge University Press)
[15] Abedi S, Slim M, Hofmann R, Bryndzia T and Ulm F-J 2016 Nanochemo-mechanical signature of organic-rich shales: a coupled indentation–EDX analysis *Acta Geotechnica* **11** 559-72
[16] Zaoui A 2002 Continuum Micromechanics: Survey *Journal of Engineering Mechanics* **128** 808-16
[17] Baird A F, Kendall J M, Fisher Q J and Budge J 2017 The Role of Texture, Cracks, and Fractures in Highly Anisotropic Shales *Journal of Geophysical Research: Solid Earth* **122** 10,341-10,51
[18] Dubey V, Mashhadian M, Abedi S and Noshadravan A 2019 Multiscale Poromechanical Modeling of Shales Incorporating Microcracks *Rock Mechanics and Rock Engineering* **52** 5099-121
[19] Sayers C, Boer L d, Dasgupta S and Goodway B 2015 Anisotropy estimate for the Horn River Basin from sonic logs in vertical and deviated wells *The Leading Edge* **34** 296-306
[20] Yu C and Shapiro S 2014 Seismic anisotropy of shale: Inversion of microseismic data. In: *SEG 2014 Annual Meeting,* (Denver: SEG) pp 2324-9